SANDIA REPORT

SAND99-2802
Unlimited Release
Printed November 1999

Laser Wire Deposition (WireFeed) for Fully Dense Shapes LDRD

Michelle L. Griffith, Mark T. Ensz, Don L. Greene, Daryl E. Reckaway, Jacob A. Morin, Thomas E. Bucheit, Thomas B. Crenshaw, David A. Lavan, Veena Tikare, and J. Anthony Romero

Prepared by
Sandia National Laboratories
Albuquerque, New Mexico 87185 and Livermore, California 94550

Sandia is a multiprogram laboratory operated by Sandia Corporation, a Lockheed Martin Company, for the United States Department of Energy under Contract DE-AC04-94AL85000.

Sandia National Laboratories

Issued by Sandia National Laboratories, operated for the United States Department of Energy by Sandia Corporation.

Available to DOE and DOE contractors from
Office of Scientific and Technical Information
P.O. Box 62
Oak Ridge, TN 37831

Prices available from (703) 605-6000
Web site: http://www.ntis.gov/ordering.htm

Available to the public from
National Technical Information Service
U.S. Department of Commerce
5285 Port Royal Rd
Springfield, VA 22161

NTIS price codes
Printed copy: A03
Microfiche copy: A01

SAND99-2802
Unlimited Release
Printed November 1999

LASER WIRE DEPOSITION (WireFeed) FOR FULLY DENSE SHAPES LDRD

Michelle L. Griffith, Mark T. Ensz
Don L. Greene, Daryl E. Reckaway, Jacob A. Morin
Mechanical Engineering Dept.

Thomas E. Buchheit, Thomas B. Crenshaw, and David A. Lavan
Mechanical Reliability and Melting Dept.

Veena Tikare
Materials and Process Modeling Dept.

J. Anthony Romero
Joining, Coating, and Net Shaping Dept.

Sandia National Laboratories
P. O. Box 5800
Albuquerque, NM 87185

Abstract

Direct metal deposition technologies produce complex, near net shape components from Computer Aided Design (CAD) solid models. Most of these techniques fabricate a component by melting powder in a laser weld pool, rastering the weld bead to form a layer, and additively constructing subsequent layers. This report will describe a new direct metal deposition process, known as WireFeed, whereby a small diameter wire is used instead of powder as the feed material to fabricate components. Currently, parts are being fabricated from stainless steel alloys. Microscopy studies show the WireFeed parts to be fully dense with fine microstructural features. Mechanical tests show stainless steel parts to have high strength values with retained ductility. A model was developed to simulate the microstructural evolution and coarsening during the WireFeed process. Simulations demonstrate the importance of knowing the temperature distribution during fabrication of a WireFeed part. The temperature distribution influences microstructural evolution and, therefore, must be controlled to tailor the microstructure for optimal performance.

Page Intentionally Left Blank.

Contents

Figures

Introduction

Laser processing has the potential for revolutionizing the rapid prototyping field to impact rapid manufacturing of metallic components. Various groups are coupling high power lasers with metal powders to fabricate metallic components, layer additively [1-4]. Typically, a laser beam is focused onto a substrate to create a molten pool into which powder particles are injected to build up each layer. The substrate is moved beneath the laser beam to deposit a thin cross section of the desired geometry. Subsequent layers are additively fabricated, thereby building a three-dimensional (3-D) component.

While metallic powders work well for the described direct metal deposition technologies, they do have drawbacks. A key aspect is material or powder utilization. Typical systems require a high-velocity spray of powder to ensure consistent material build up; however, only a small amount of the powder is actually retained in the molten pool, approximately 20%. In the WireFeed process, powder is replaced with wire feedstock to fabricate components. With wire feedstock, 100% utilization is achieved during fabrication, because all wire injected into the molten pool is used to fabricate the part. Therefore, no recycling system is required; and faster build times can be accommodated. Furthermore, uniform flow of the powder material is crucial to successful fabrication in laser/powder technologies, where control can be difficult to maintain. It is relatively simple to maintain constant wire feed rates. Another consideration is availability of material; many materials are readily available in wire form. Direct metal deposition with powder feedstock requires a good powder source, where size distribution and composition must be carefully controlled. This report describes the WireFeed process, the resultant material properties for as-processed 308L and 304L stainless steel, and modeling results of the microstructural evolution.

WireFeed Process

Figure 1 shows a schematic of the initial prototype WireFeed system. The system consists of a CW 600W Nd:YAG laser, a 4-axis computer-controlled positioning system, and a wire feed unit [5]. The positioning system and wire feed unit are mounted inside a box with localized gas purge capability. During fabrication, the workpiece and surrounding area are purged with argon to minimize oxidation of the workpiece. The laser beam is brought into the box through a window mounted on the top of the box and directed to the deposition region using a six-inch focal length lens. The wire feed unit is designed to inject the wire into the molten pool from one side, and the lens and wire feed unit move as an integral subsystem.

Geometries are written into a series of tool path patterns to build each layer. This file is combined with other commands to drive the laser, the positioning stages, and the wire feed unit to produce the desired component one layer at a time, starting from the bottom of the part. A solid substrate is used as a base for building the WireFeed object. The laser beam is focused onto the substrate to create a weld pool (~1mm diameter) in which typically 250-micron diameter fine wire is injected. The substrate is moved beneath the laser beam to deposit a thin cross section, thereby creating the desired geometry for each layer. After deposition of each layer, the wire feed mechanism and focusing assembly are incremented in the positive Z-direction, building a three dimensional component layer additively.

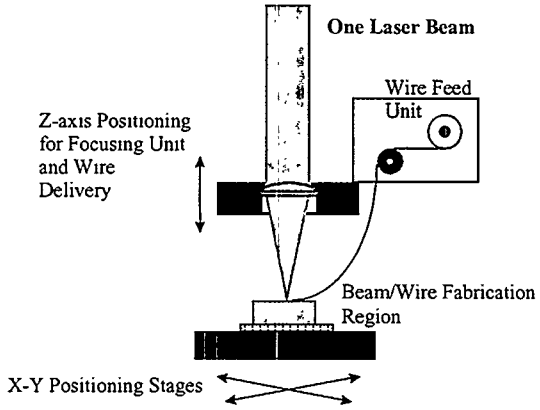

Figure 1. Schematic of the prototype WireFeed system showing the laser perpendicular to the substrate and wire feed from side.

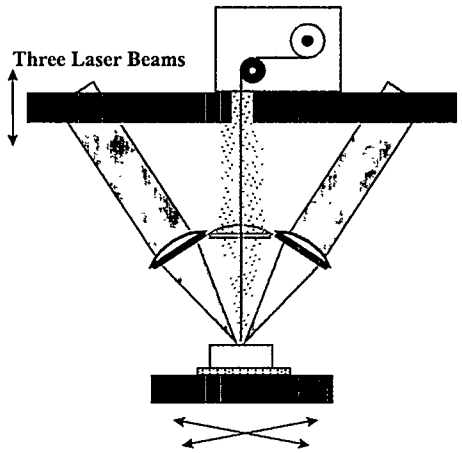

Figure 2. Schematic of the improved system with three laser beams at 120° placement surrounding wire.

Shape Fabrication

Initially, test matrices were developed and implemented to identify the key factors controlling the WireFeed process. From previous work [6], laser power, material rate,* and traverse velocity are the key factors to control deposition in direct metal fabrication. Along with those tests, extra experimental studies were required to understand the relationship between the wire and the weld pool for the system shown in Figure 1. This study included varying the wire feed direction, wire feed height (w.r.t. the substrate), and insertion angle. Diagnostic tools, such as video camera techniques (high speed and magnification), were used to monitor and understand the wire/molten pool interaction.

Because of these studies, the wire must intersect the molten pool in such a manner to maintain stability along the solidification front. If the wire is inserted too high (w.r.t. the substrate or previous layer), it does not remain connected with the pool; if the wire is inserted too low, the wire either stubs on the substrate/layer or is pushed around by the force of the weld pool. After choosing the intersection point, the insertion angle and direction must be determined. An insertion angle of 45 degrees maintains the best stability, and uniform deposition is only maintained with wire insertion perpendicular to the deposition direction. The consistency of build is not maintained if the wire is inserted either from the trailing or leading edge of the weld pool, because the molten pool has difficulty forming and maintaining the bead as the source material or energy moves away.

Since the process was highly dependent on the position of the wire in relation to the deposition direction, a new system was configured to remove this geometric processing constraint. As

* Material rate is powder flow rate for Reference 6 and is wire feed rate for this report.

shown in Figure 2, the wire is fed down the center and the laser beam is split into three beams (by use of fiber optics) to surround the wire. The laser heads are stationed 120 degrees apart from each other. Now, the wire always enters the pool at the "hot spot," and constraints do not exist on direction of travel. This new design was imperative for complex part fabrication.

From the process variable experiments, the laser wire deposition parameters were optimized to demonstrate feasibility of part fabrication. Test matrices were added to understand how layer thickness and hatch (fill) spacing affected part fabrication. In order to control the wire feed during layer increments for simple block shapes, process studies were conducted. After a layer is fabricated in a serpentine raster pattern, the laser shutter closes, and the focusing and wire feed subsystems must increment in the positive Z direction to fabricate the next layer. Before the Z increment, the wire must reliably detach from the part. Consistent detachment of the wire from the molten pool is possible through a specific timing procedure, where the wire is retracted from the molten pool before the laser energy is removed. This knowledge is required for complex part fabrication with increasing area complexity.

Various shapes with increasing complexity are shown in Figure 3. Currently, three standard types of geometries have been fabricated:

1. unidirectional fabrication using a rotary stage to build hollow cylinders (Figure 3a),
2. bidirectional patterns to fabricate walls, and
3. with an understanding of wire detachment, hatch spacing and layer thickness, it was possible to fabricate dense, rectangular solids from 308L stainless steel (Figure 3b).

We initiated complex part fabrication with the challenge of building two cubes (Figure 3c), where the raster pattern jumps back and forth between the cubes to deposit the lines of each cube layer, with a multitude of connect/disconnect sequencing of the wire and weld pool in each layer.

With control of the deposition process in the layer as well as subsequent layers, we have fabricated more complex shapes such as the nozzle-cone shape shown in Figure 3d. This was only possible with the new WireFeed system design shown in Figure 2. All shapes possess 100% utilization of the wire, where the material inserted into the molten pool is directly used to produce a part. WireFeed parts are quickly fabricated, between 0.5-1.0 hour per cubic inch.

Typical processing parameters are:

- Laser power: 300 – 400 Watts
- Traverse velocity: 6.4 – 8.5 mm/s (15-20 in/min)
- Wire feed rate: 32 – 53 mm/s (75-125 in/min)
- Line spacing: 500 – 750 microns (0.020" – 0.030")
- Layer spacing: 500 – 750 microns (0.020" – 0.030")

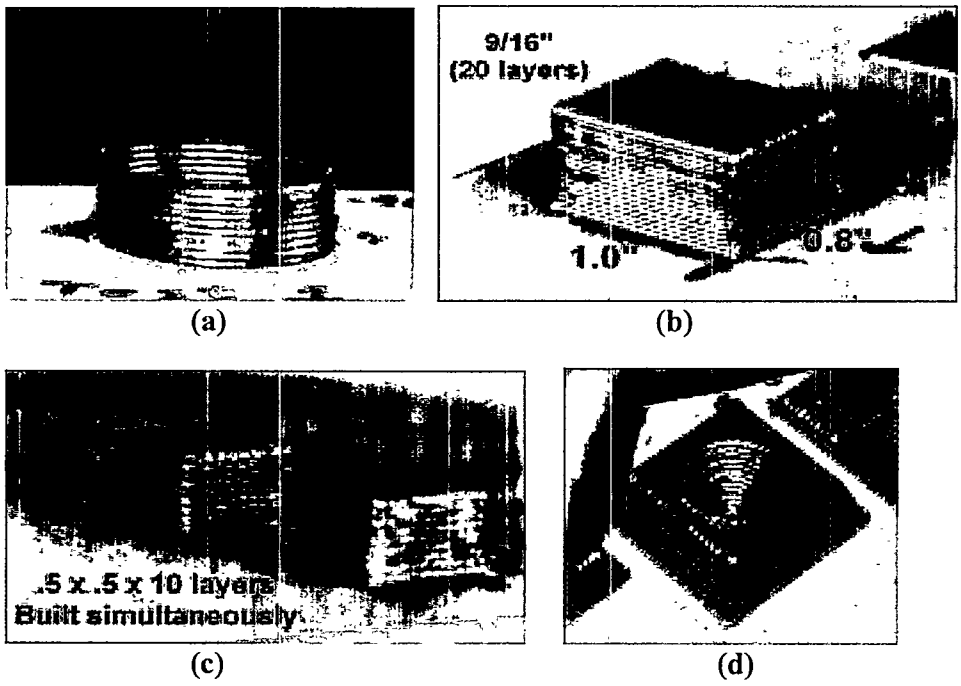

Figure 3. (a) unidirectional fabrication of hollow cylinder, (b) block fabrication with wire detachment between layers, (c) complex part fabrication with start- and stop-capability in each layer, and (d) complex geometry fabrication of nozzle-cone.

Materials Characterization

Microstructures

Metallographic analysis was used to study the deposition process and the resulting microstructures formed by the WireFeed process. Figure 4 is a micrograph to show a given set of parameters could produce nearly defect free parts, where most passes produce the correct fusion to knit the lines and layers together.

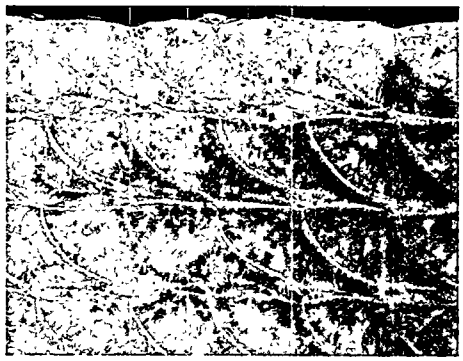

Figure 4. Micrograph showing deposition cross-section for 308L stainless steel in the WireFeed process (32X magnification).

Further metallographic analysis within these lines revealed dense, fine grain microstructures for 308L stainless steel produced by the WireFeed process as shown in Figure 5. Figure 5(a) is a cross-sectional view of a line drawn by the WireFeed process. Typical microstructural features are small, on the order of 4 microns, because of the high solidification rate in the WireFeed process. Figure 5(b) is a top view showing one full line and two partial lines (interfaces between lines marked at A). The fine microstructural features show directional solidification behavior resulting in textured features. Later in this report, we will describe our efforts to model these features and the effect of processing parameters on resultant microstructures.

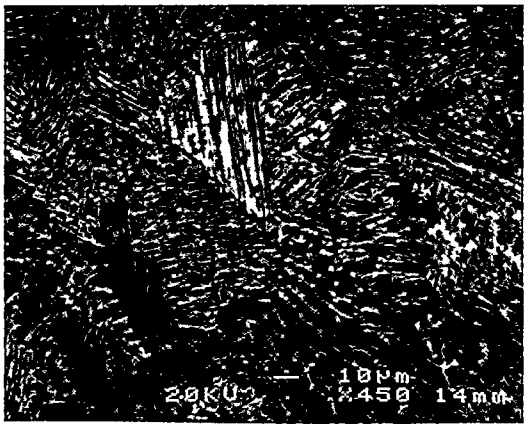

(a)

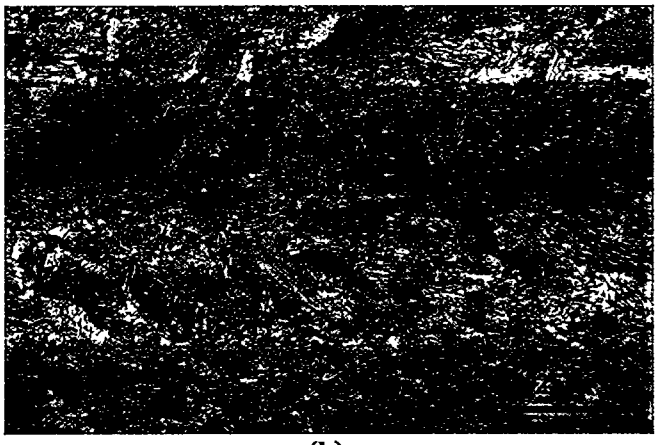

(b)

Figure 5. Typical microstructures for 308L stainless steel, where (a) is a view inside a fabrication line (450x magnification) and (b) is a view of three lines fabricated in a layer (laser rastered from right to left).

General Mechanical Behavior

Coupons were machined from the as-processed 308L stainless steel for room temperature tensile testing, where the pull direction is parallel to the build plane in the WireFeed sample (longitudinal). All samples had densities greater than 98%. The results for WireFeed-processed

material are compared to typical annealed material in Table 1. With grain size refinement, the WireFeed material possesses strengths greater than annealed, where the yield strength is 58 ksi as compared to 35 ksi for the annealed material. However, the ductility remains consistent with elongation values of 65-75%, which are slightly higher than the annealed values (55-65%). High strengths and hardness with retained ductility are a good combination for WireFeed-processed material.

Table 1. Room temperature mechanical properties for as-processed 308L stainless steel compared to typical annealed material.

Property	WireFeed longitudinal	Annealed material
Hardness	87 HRB	80 HRB
Microstructure feature size	4 Micron	40 Micron
Tensile strength (Yield)	58.2 ksi	35 ksi
Tensile strength (Ultimate)	94.2 ksi	85 ksi
Ductility (Elongation)	64.9%	55%
Ductility (Reduction in area)	74.6%	65%

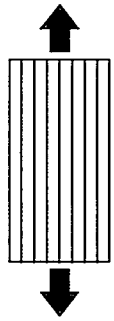

The effect of deposition style was studied for 304L stainless steel material. Two types of patterns were fabricated: (1) longitudinal and (2) cross hatch where every other layer is deposited 90 degrees to the previous layer. Table 2 shows the results. Both deposition patterns show similar strength properties, with yield values much greater in comparison to annealed material. However, there is a trade-off with a decrease in ductility, especially for the cross hatch pattern style. Any flaws in adhesion between layers would be more evident in the cross hatch samples because the weak layers are perpendicular to the tensile pull direction. Overall, the material properties for these stainless steel alloys show benefit in strength values compared to traditional annealed material, and in some cases the ductility is nearly maintained.

Table 2. The effect of deposition pattern on room temperature mechanical properties for as-processed 304L stainless steel.

Property	Longitudinal Pattern	Cross Hatch Pattern	Annealed 304L
Tensile strength (Yield)	75.9 ksi	76.1 ksi	42.8
Tensile strength (Ultimate)	104.2 ksi	102.0 ksi	95.9
Ductility (Elongation)	48.3%	34.6%	56.0
Ductility (Reduction in area)	40.0%	32.8%	---

Mechanical Behavior of Microsamples

From the previous section, it became important to understand the effect of bead interfaces, or adhesion between deposition lines, on the resulting material properties. This is possible by testing miniature samples that study the strength extremes in WireFeed fabrication. At one

extreme, longitudinal samples consist of nearly single line fabrication with few, if any, interfaces to study the theoretical strength properties. The other extreme consists of tranverse samples that contain many line interfaces to study the bead-to-bead adhesion on resulting material properties. Miniature samples of material cut from a 308L stainless steel rectangular block were tested using a small-scale tensile test machine built at Sandia [7]. Much of the procedure was in accordance with ASTM standards as possible; standards for miniature tensile testing do not exist. This test technique has been used for several studies of LIGA-deposited materials for MEMS [8, 9]. Load is applied with a small servo-hydraulic unit, which is digitally controlled. Load is measured using a 225N (50 lb) load cell, and strain is measured on the sample using a scanning laser extensometer. Cross-head displacement is also measured using a micro LVDT. Samples were cut using a wire-EDM in a two-step process. First, several 400 μm (.016") thick slices were cut and polished to a 600-grit finish using standard metallographic techniques. Second, the slices were stacked together, and the miniature tensile samples were cut in groups of three using the wire-EDM to trace the outline of the samples. Half of the samples were cut in the longitudinal directional (with the motion of deposition), while the rest were in the transverse direction. The gauge cross section is roughly 760 μm wide by 350 μm thick. Each sample was measured before testing.

The longitudinal samples provided very consistent results. The average and standard deviation for six samples is:

- yield 62.4 ± 2.6 ksi,
- ultimate 92.5 ± 1.9 ksi, and
- total elongation of 41± 5%.

The strength and elongation of the transverse samples were not as good, where regions of poor fusion reduced the ultimate strength and severely reduced the total elongation:

- yield 58.5 ± 5.1 ksi,
- ultimate 70.2 ± 11.5 ksi, and
- total elongation of 8.6 ± 9.9%.

A summary of all the tests is provided in Table 3.

The consistency in the longitudinal samples is expected, because in most cases, each sample represents one line of deposition in the WireFeed process. Therefore, the strength properties should be near the theoretical equivalent for the material. By comparison to the properties measured in Table 1, the strength properties match closely for samples that consist of many line and layer depositions, and therefore show the inherent strength in WireFeed-processed material.

For transverse samples, each microsample consists of approximately 3-5 layers of deposition in the gauge section. As shown in Table 3, any difficulties with fusion between layers will result in poor properties. This is especially true for the ductility values (elongation %), where any imperfections will result in premature fracture.

Table 3. Tensile properties of WireFeed 308L stainless steel tested using microsamples.

Sample ID	0.2% Yield (ksi)	Ultimate (ksi)	Elongation (%)
Longitudinal 1-1	57.9	90.5	47
Longitudinal 1-2	61.4	90.4	43
Longitudinal 1-3	63.2	93.5	43
Longitudinal 2-1	62.1	92.7	41
Longitudinal 2-2	63.8	92.8	34
Longitudinal 2-3	65.4	95.3	38
Average Long.	**62.4 ± 2.6**	**92.5 ± 1.9**	**41 ± 5**
Transverse 1-1	62.2	76.6	10
Transverse 1-2	64.8	90.6	28
Transverse 1-3	58.5	65.7	4.3
Transverse 2-1	53.1	62.5	2.9
Transverse 2-2	51.8	60.0	3.8
Transverse 2-3	60.2	65.4	2.3
Average Trans.	**58.5 ± 5.1**	**70.2 ± 11.5**	**8.6 ± 9.9**

SEM micrographs of the fracture surface of the tensile samples illustrate the difference between the transverse and longitudinal test samples. Figure 6 is the fracture surface of a longitudinal sample that shows classic necking and ductile dimple rupture. Figure 7 is a fracture surface of a transverse sample that failed at a region between deposition passes where there was lack of fusion.

It was determined that this lack of fusion was related to the starting wire, not the processing parameters. The cleanliness of the wire had a direct result on the properties. If the wire is not properly cleaned after the drawing process, residual oils and other contaminants are incorporated into the final product. These contaminants become glassy phase particles that act as porosity centers or high-stress concentration sites. In these microsamples, any small defect will result in poor properties on this scale.

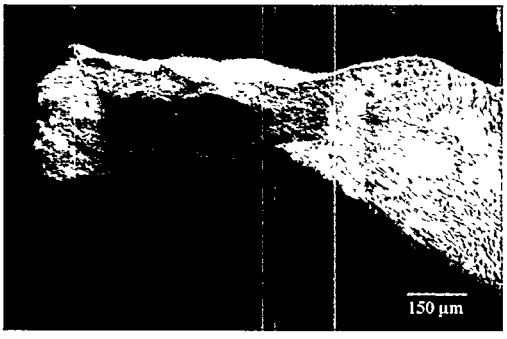

Figure 6. Typical longitudinal sample.

Figure 7. Typical transverse sample showing a lack of fusion region.

Simulation of Coarsening in WireFeed Microstructures

Background

This fabrication process results in microstructures that are unique. Each deposited line has features inherent to it. Some features extend into the neighboring lines and into the adjoining layers as shown in Figure 5. These features such as grain size and shape have a large effect on material properties and performance. Therefore, it is essential that microstructural evolution during fabrication be controlled. To this end, we are developing a model to predict microstructural evolution during fabrication. In this report, we present a model capable of simulating coarsening in a single-phase system under an assumed temperature profile.

A kinetic Monte Carlo model, known as the Potts model [10], was used to simulate coarsening during the WireFeed process. The Potts model has enjoyed great success in simulating and predicting many evolving microstructures including normal grain growth, abnormal grain growth, recrystallization, Ostwald ripening, pore migration, etc. In this work, we adapt it to the spatial and thermal conditions experienced during the WireFeed process.

Two-Dimensional Coarsening Simulations

Simulation method

The Potts model was adapted to simulate two-dimensional coarsening in the dynamic temperature profile of the rastering laser used by the WireFeed process. Microstructural representation in the Potts model is done by populating a lattice with a canonical ensemble. We use a square lattice and each lattice site is assigned a "spin."[†] Contiguous sites of the same spin form a grain with a sharp grain boundary between adjacent grains. The number of different, degenerate spins that the lattice sites can assume is Q. The individual state is designated by the symbol q and the total number of states in the system is Q, $q_{grain} = [1, 2, \ldots Q]$. All the simulations in this work used $Q = 100$. The equation of state is the sum of all the neighbor interaction energies in the system given by

$$E = \frac{1}{2} \sum_{i=1}^{N} \sum_{j=1}^{8} \left(1 - \delta(q_i, q_j)\right) \qquad (1)$$

where

N is the total number of sites,
δ is the Kronecker delta with $\delta(q_i = q_j) = 1$ and $\delta(q_i \neq q_j) = 0$,
q_i is the state of the grain at site i and
q_j is the state of the nearest neighbor at site j.

[†]The term spin originates from the original application of the Potts model that was used to study domain growth in magnetic materials.

Thus, the only energy considered in the simulation is the interfacial energy and all unlike neighbors contribute one arbitrary unit of energy to the system. This yields a single-component, single-phase system with uniform, isotropic [11] interfacial energies between grains.

Now that the microstructural representation and system energies are defined in the simulation, we turn to grain growth mechanism and kinetics. Grain growth is simulated using the method developed in previous works [12, 13]. First, a grain site is chosen at random from the simulation space. Then a new state q is chosen at random from the Q possible states in the system. The grain site is temporarily assigned the new state and the change in energy is evaluated using Equation 1. Next the standard Metropolis algorithm is used to perform the grain growth step based on Boltzmann statistics. A random number, R, between 0 and 1 is generated. Next, the transition probability, P, is calculated using

$$P = \begin{cases} \exp\left| \dfrac{-\Delta E}{k_B T} \right| & for \quad \Delta E > 0 \\ 1 & for \quad \Delta E \leq 0 \end{cases} \tag{2}$$

where

k_B is the Boltzmann constant and
T is absolute temperature.

If the $R \leq P$, then the grain growth step is accepted; if not, the original state is restored. The simulation temperature used for grain growth, $k_B T = 0$, has been shown to simulate grain growth well. Time in the Potts model is measured in units of Monte Carlo step; 1MCS corresponds to N attempted changes, where N is the total number of sites in the system.

In order to simulate the WireFeed process, the Potts model was modified to include a dynamic temperature profile. This was done by considering the grain boundaries to have a velocity, V_{gb}, which is proportional to grain boundary mobility, M_{gb}, and to the driving force, μ, as

$$V_{gb} = M_{gb}\mu \tag{3}$$

Assuming that the mobility of the grain boundaries is a function of temperature, one can simulate coarsening in a dynamic temperature environment by using a temperature dependent mobility term, $M_{gb}(T)$. At high temperatures, the mobility term is large and at lower temperatures it is small. Since we are simulating a laser beam rastering across a part, the mobility term becomes a function of position, x, and of time, t, $M_{gb}(x,t)$. The transition probability given in Equation 2 is modified to include temperature dependence by multiplying the mobility term as

$$P = M_{gb}(x,t)\begin{cases} \exp\left|\frac{-\Delta E}{k_B T}\right| & for \quad \Delta E > 0 \\ 1 & for \quad \Delta E \le 0 \end{cases} \tag{4}$$

The temperature profile assumed for the WireFeed process is a laser beam with a Gaussian temperature distribution, representing the WireFeed system shown in Figure 1. All modeling results assume this system configuration. Preliminary characterization of the laser beam indicated that the beam was elliptically shaped; thus, a Gaussian distribution as shown in Figure 8 was used for the simulation. Grain growth in a single line width and of an arbitrary length was simulated in this work with a temperature profile, as shown in Figure 8, rastered across the length of the line.

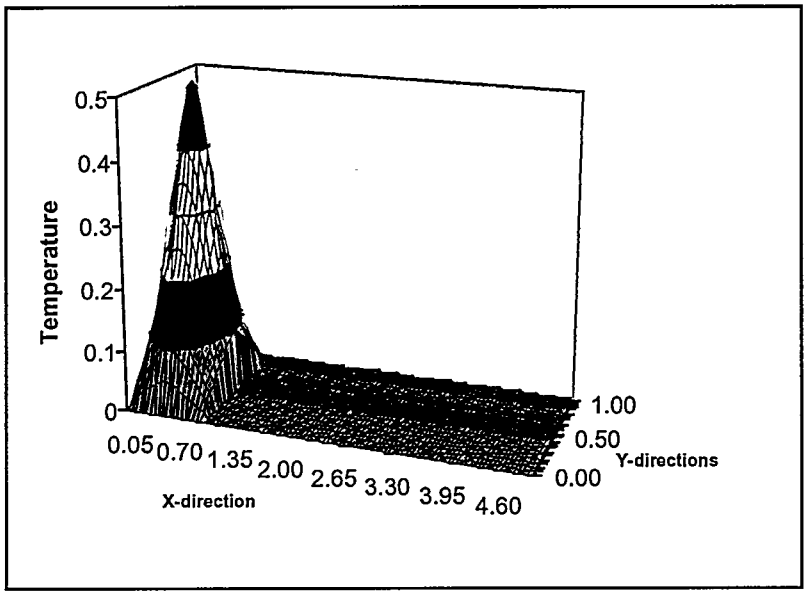

Figure 8. The temperature profile with Gaussian distribution in the X- and Y- directions was used to simulate coarsening.

2-D simulation results

Microstructures resulting from simulations of coarsening under a rastering temperature profile of a laser beam are shown in Figures 9 and 10 for two laser beam velocities, V_{lb}= 0.05 and V_{lb}= 0.001 sites/MCS. At the higher temperatures in the center of the line, grains have grown larger. At the faster laser velocity V_{lb}= 0.05 sites/MCS, the grains are slightly elongated in the center. However, the microstructure is dramatically different at the slower raster velocity with highly elongated grains in the central high-temperature region. The grains in the cooler region are progressively less elongated and become equiaxed at the coolest region. By comparison to Figure 5 (b), the WireFeed microstructure best resembles the slower velocity model, where the grains are more elongated. However, this 2-D model does not accuractely describe the direction

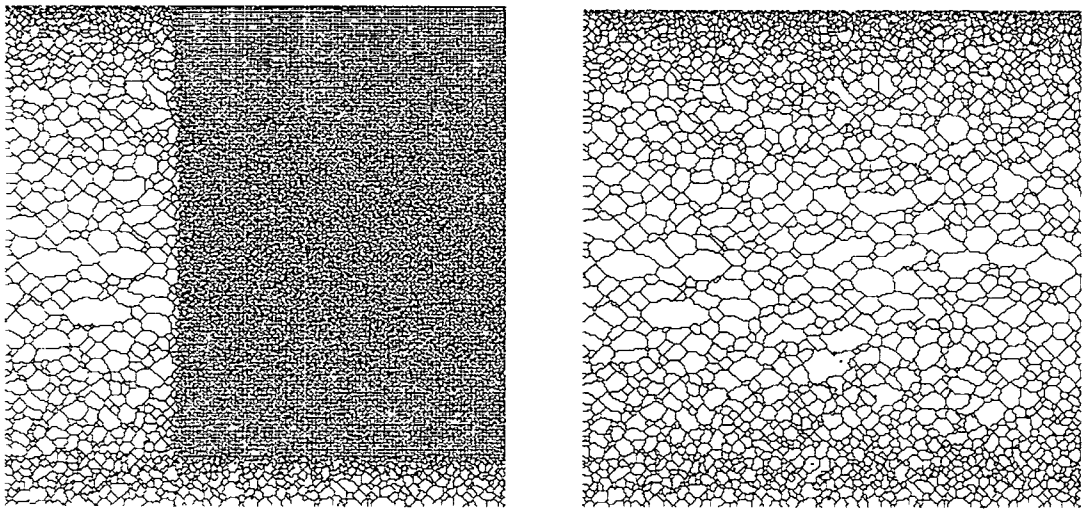

Figure 9. Coarsening in a deposition layer at mid- and full-raster of a laser beam. The raster velocity, V_{lb} = 0.05 sites/MCS. The laser raster direction is to the right. The strip at the bottom of the figure is the previously deposited line.

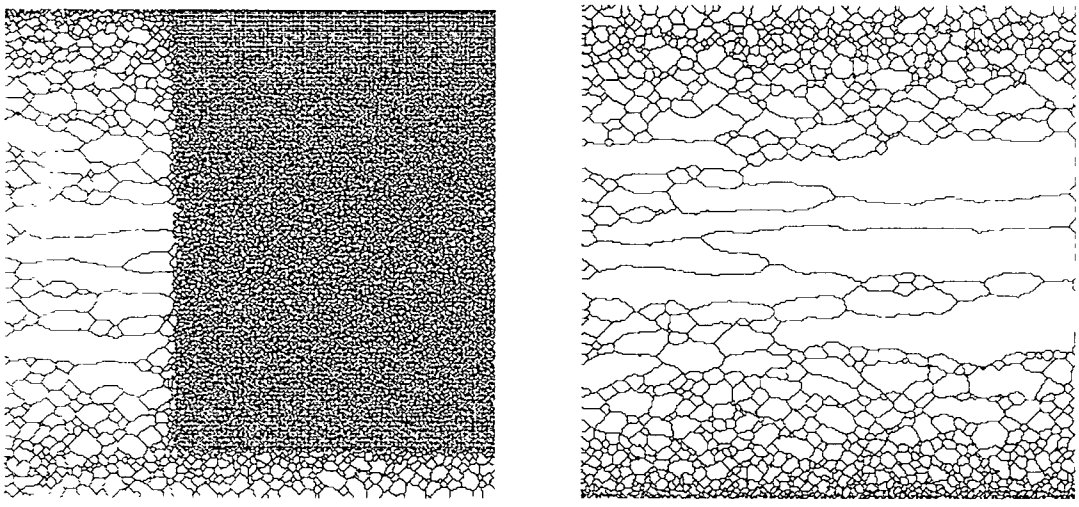

Figure 10. Coarsening in a deposition layer at raster velocity, V_{lb} = 0.001 sites/MCS. The raster direction is to the right and strip is previously deposited line.

of the elongated grains. Actual microstructures show elongated and texture where the grains and other features are slightly off-axis as one would expect in a weld-type operation, such as this technology.

As a result of the good but not accurate prediction of grain morphology, it was necessary to investigate the profile of the laser beam to obtain a more accurate thermal profile. Preliminary characterization of the laser beam in the WireFeed apparatus (Figure 1) revealed that the elliptical Gaussian shape of the laser beam was not perpendicular to the laser raster direction, but slightly rotated about the axis as shown in Figure 11. To understand the effect of such a laser beam, we ran simulations with a rotated beam. All other simulation parameters were the same as the previous simulation (Fig. 10). As shown in Figure 12, the grain morphology follows the change in the beam shape. The abrupt change in microstructure at the left end is due to the use of periodic boundary conditions and is not seen in real WireFeed parts. The results presented in this section have been published [14].

In summary, the 2-D simulations show that the traverse velocity reasonably predicts the size of the grains for WireFeed processing, but does not accurately describe the texture of the morphology. The thermal profile of the laser beam and resultant thermal profile in the WireFeed part must be better described to accurately predict microstucture.

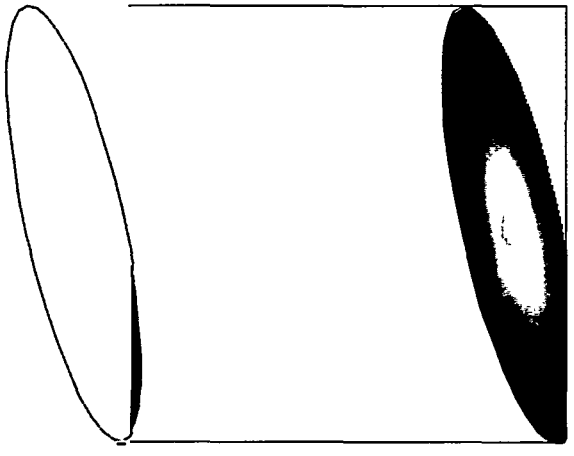

Figure 11. The temperature distribution across the simulation space with a periodic boundary condition at time t = 0.

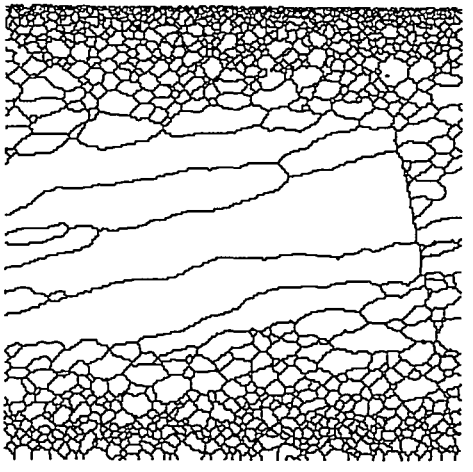

Figure 12. Grain growth with a tilted temperature distribution.

Three-dimensional coarsening simulations

Simulation method

The simulations were extended to 3-D by digitizing on a cubic lattice. Like the 2-D model, grains could assume one of $Q = 100$ spins. The equation of state is the same as that in Equation 1, except in 3-D, interactions with the 26 first, second, and third nearest neighbors are summed.

Again, the rastering temperature profile is simulated by taking the mobility to be a function of temperature as given by Equation 3.

The temperature profile used in the simulations is the Rosenthal solution to a moving point source of heat given by:

$$T_m - T = \left(\frac{\alpha Q}{2\pi k r_p} \right) \exp\left(\frac{-C}{2k} (x_p + r_p) \right) \tag{5}$$

where

T_m is melting temperature,
T is temperature at r_p.
The distance for the center of the laser spot and x_p and the distance from the laser spot along the direction of travel and are:

$$r_p = \sqrt{(x_p - vt)^2 + y^2 + z^2} \qquad \text{and} \qquad x_p = x - vt \text{ and}$$

x is the laser travel direction,
z is depth, vt is the current laser position along the x-direction,
α is the heat transfer efficiency,
Q is heat input, k is conductivity, and
C is heat capacity.

The temperature profile at the surface is shown in Figure 13.

In the 3-D simulation, the deposition of two layers, one on top of the other, was simulated. First, deposition of layer with the Rosenthal temperature profile is simulated. Next, deposition of a second layer over the first layer so that the microstructure is contiguous with the layer below is simulated.

3-D simulation results

The results of the 3-D simulations are shown in Figures 14 and 15, with simulated microstructures of grains after a laser has passed across at velocity v = .02 and v = .01 sites/MCS, respectively. Features of the same shades are grains. The microstructures show that the grain grew faster in the center region, which is the hottest area, and much slower at the outside cooler region as was expected because grain boundaries have higher mobility at higher temperatures. The elongation of the grains was dependent on the velocity of the laser. At slower laser velocity, grains are highly elongated as the grain boundary mobility is able to keep pace with the laser. At high laser velocity, the grains were smaller and less elongated because the laser velocity was faster than the grain boundary mobility. Furthermore, the direction of grain elongation was perpendicular to the Rosenthal isotherm as seen in Figure 13.

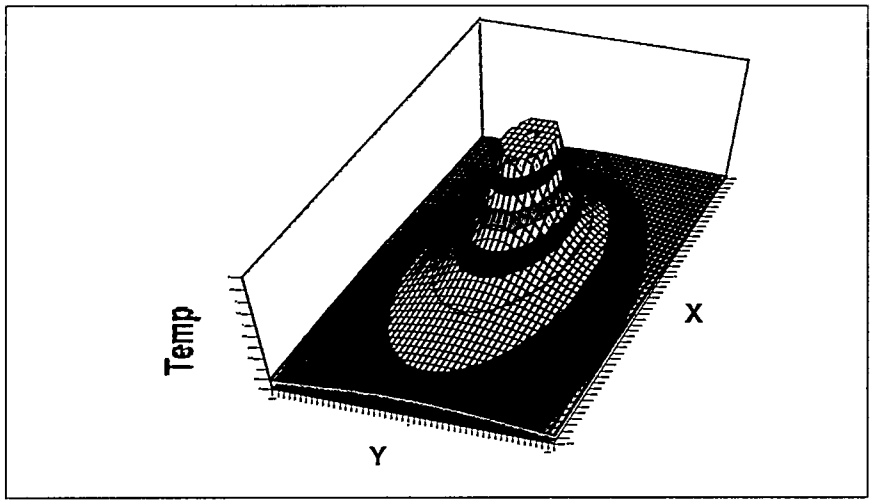

Figure 13. Rosenthal temperature profile at the surface, with heat source moving along the X-direction.

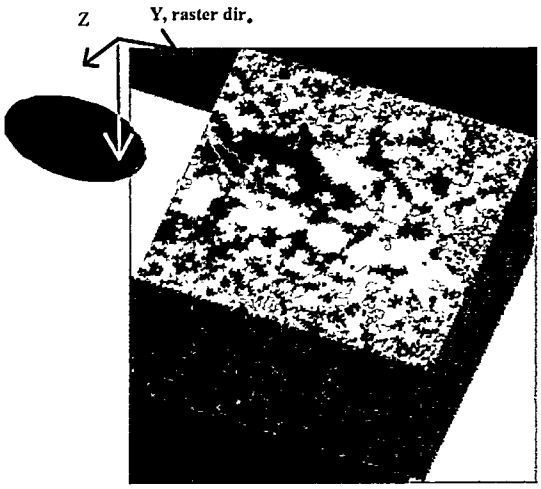

Figure 14. Microstructure after deposition of the first layer at laser velocity v = 0.02 st/MCS.

Figure 15. Microstructure after deposition of the first layer at velocity v = 0.01 st/MCS.

The microstructural evolution of the first layer after deposition of both layers is shown in Figure 16 (a) and 16 (b). As one can see, the first layer has continued to coarsen during deposition of the layer above it.

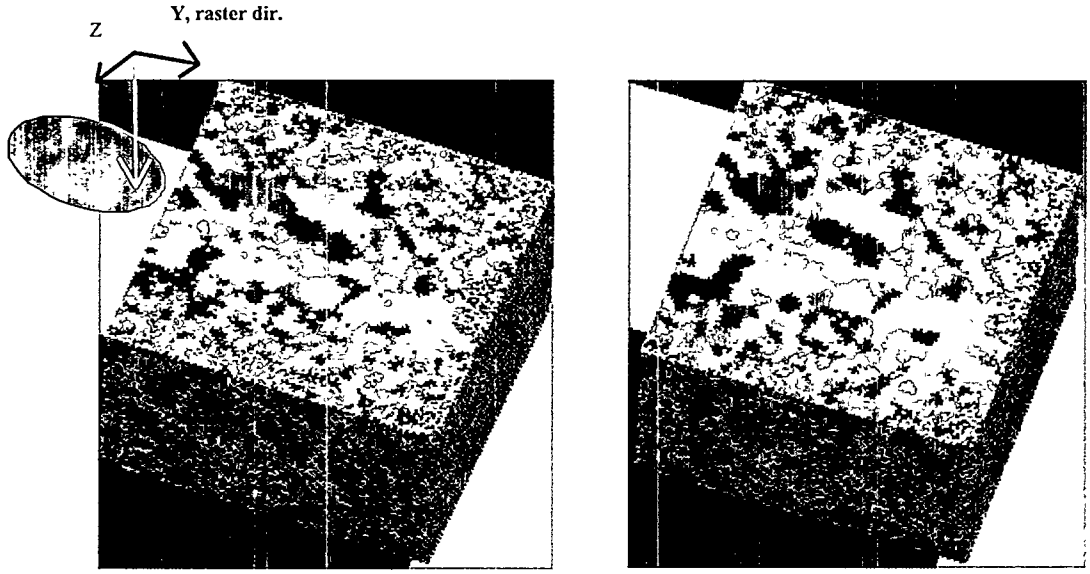

Figure 16. Microstructure of the first layer after (a) initial depostion of the first layer and (b) deposition of the second layer.

Initial comparison between the 3-D model microstructures and experimental structures shows a reasonable correlation as seen between Figure 5(b) and Figure16. The direction of grain growth along the laser path is seen in both figures, and the relative size and relation of grains is similar. Future work will focus on better correlation between the model, temperature profile description, process parameters, and resulting microstructures.

Discussion

The Potts model has been used extensively to study many different coarsening phenomena. However, incorporating a dynamic, non-linear temperature in the Potts model to simulate coarsening in a WireFeed part during fabrication is a unique application of this model. In this work, simulation of coarsening in a dynamic temperature environment was achieved by varying the mobility of the grain boundaries with temperature. This is an accurate modeling method as long as the grain growth mechanism and driving force for grain growth are temperature independent and only grain-boundary mobility changes with temperature. This is a valid assumption as the growth mechanism and driving force for a number of thermally activated processes is temperature independent over fairly large temperature ranges. Furthermore, in the current study, we were not interested in the effects of multiple grain-growth mechanisms or temperature-dependent driving force on coarsening. The objective here was to understand coarsening in single-phase isotropic, material subject to an unusual thermal history.

The simulations presented in this report show that the raster speed of the laser energy and the temperature distribution around it have a large effect on the grain size and shape. At the faster laser raster speed, the grains were slightly elongated in the hot section. At this speed, the grain boundary velocity was too slow to grow with the laser beam. When the laser raster speed was slowed, the grain boundary velocity was able to move with the laser. In the cooler regions, the

grain boundary velocity was slower; thus, unable to move with the laser energy. This resulted in progressively smaller, more equiaxed grains away from the high temperature region of the simulation. The elongation of the grains was perpendicular to the isotherms of the temperature profile as shown by Figures 9-12 and 14-16.

The simulations in this work demonstrate the importance of knowing and controlling the temperature distribution during fabrication of a WireFeed part. The temperature distribution influences microstructural evolution and, therefore, must be controlled to tailor the microstructure for optimal performance. Conversely, if certain microstructural features are desirable, this simulation capability can be used to determine the temperature profile necessary for their formation.

Conclusions

This report described a new direct metal deposition process, known as WireFeed [15], to fabricate dense metal parts directly from a CAD solid model. Initially, much effort was required to understand and control the deposition of the wire. It became necessary to redesign the system [16] to reliably feed the wire into the molten pool. This permitted the project to move forward for fabrication of complex geometries, including the nozzle-cone shape.

Complementary to deposition for shape control, the project obtained an understanding of the material properties that result from the WireFeed process. Parts were fabricated from two grades of stainless steel—304L and 308L—where the strength properties were enhanced by the fine microstructural features formed from the high cooling rates during deposition. In most cases, the ductility was maintained without sacrificing strength properties—a good match. It is important to ensure the cleanliness of the wire feedstock in order to maintain the integrity of the properties for all parts.

Simulations demonstrate the importance of knowing and controlling the temperature distribution and velocity during fabrication of a WireFeed part. The temperature distribution and velocity influences microstructural evolution and, therefore, must be controlled to tailor the microstructure for optimal performance.

References

1. M. L. Griffith et al., "Free Form Fabrication of Metallic Components using Laser Engineered Net Shaping (LENS)," Solid Freeform Fabrication Symposium Proceedings, August 12-14, 1996, Austin, TX, p.125.

2. J. R. Fessler et al., "Laser Deposition of Metals for Shape Deposition Manufacturing," Solid Freeform Fabrication Symposium Proceedings, August 12-14, 1996, Austin, TX, p. 117.

3. F. Klocke, H. Wirtz, and W. Meiners, "Direct Manufacturing of Metal Prototypes and Prototype Tools," Solid Freeform Fabrication Symposium Proceedings, August 12-14, 1996, Austin, TX, p.141.

4. J. Mazumder et al., "The Direct Metal Deposition of H13 Tool Steel for 3-D Components," JOM, Vol 49, Number 5 (1997), p. 55.

5. E. Brandon, F. Hooper, and M. Reichenbach, "Precision Wire Feeder for Small Diameter Wire" (U. S. Patent #5137223, August 11, 1992).

6. D. M Keicher et al., "Towards a Reliable Laser Powder Deposition System through Process Characterization," Proceedings of SAMPE '95, Albuquerque, NM, October 12-14, 1995, p. 1029.

7. Schmale, David T., Roy J. Bourcier, Thomas E. Buchheit, "Description of a Micro-Mechanical Testing System," Sandia National Laboratories SAND97-1608, July 1997.

8. Christenson, T.R.; T. E. Buchheit, D. T. Schmale, R. J. Bourcier, "Mechanical And Metallographic Characterization Of LIGA Fabricated Nickel And 80%Ni-20%Fe Permalloy," Proceedings of the 1998 MRS Spring Symposium April 15-16, 1998, v 518 San Francisco, CA, pp. 185-190.

9. Buchheit, T.E., T.R. Christenson, D.T. Schmale, and D.A. LaVan, "Understanding And Tailoring The Mechanical Properties of LIGA Fabricated Materials," Proceedings of the 1998 MRS Fall Symposium Dec 1998, Boston, *in publication.*

10. F. Y. Wu, "The Potts Model," Rev. Modern Phys., 54 [1] 235-268 (1982).

11. E.A. Holm, James A. Glazier, D.J. Srolovitz, G.S. Grest, "Effects of Lattice Anisotropy and Temperature on Domain Growth in the Two-Dimensional Potts Model," Phys. Rev. A, 43 [6] 2662-2668 (1991).

12. D.J. Srolovitz, G.S. Grest, M.P. Anderson, and A.D. Rollett, "Computer Simulation of Recrystallization II. Heterogeneous Nucleation and Growth," Acta Metall., 36 [8] 2115-2128 (1988).

13. J. Wejchert, D. Weaire, J.P. Kermode, "Monte Carlo Simulation of the Evolution of a Two-Dimensional Soap Froth," Phil. Mag. B53 15-24 (1986).

14. V. Tikare, M.L. Griffith, E. Schlienger, J.E. Smugeresky, "Simulation of coarsening during laser engineered net-shaping", Proc. 8th Solid Freeform Fabrication Sympsium, August 11-13, 1997.

15. M. L. Griffith, M. T. Ensz, D. L. Greene, D. E. Reckaway, J. A. Romero, T. B. Crenshaw, L. D. Harwell, T. E. Buchheit, and V. Tikare, "Solid Freeform Fabrication using the WireFeed Process," Proceedings of the Solid Freeform Fabrication Symposium, August 1999, Austin, TX, in press.

16. L. Harwell, M. Griffith, D. Greene, G. Pressly, "Energetic Additive Manufacturing Process with Feed Wire," Patent Application #09/076402, filed 5/12/1998.

Distribution:

10	MS0958	Michelle L. Griffith, 1484
1	MS0958	Mark T. Ensz, 1484
1	MS0958	Don L. Greene, 1484
1	MS0958	Daryl E. Reckaway, 1484
1	MS0333	Thomas E. Buchheit, 1835
1	MS1407	David A. Lavan, 1835
1	MS0367	Thomas B. Crenshaw, 1835
1	MS1411	Veena Tikare, 1834
1	MS0340	J. Anthony Romero, 1833
1	MS1411	Joe Puskar, 1833
1	MS0958	Clint Atwood, 1484
1	MS 1411	Duane Dimos, 1843
1	MS0958	Bruce Swanson, 1484
1	MS0960	Jimmie Searcy, 1400
1	MS9018	Central Technical Files, 8940-2
2	MS0899	Technical Library, 4916
1	MS0612	Review & Approval Desk, 4912 For DOE/OSTI
1	MS0188	LDRD Office, 4001

Page Intentionally Left Blank.